Stress Analysis and Thermal Characterization of a High Pin Count PQFP

A. Mertol
LSI Logic Corporation,
Fremont, CA 94539
Mem. ASME

A three-dimensional finite element model of a high pin count plastic-quad-flat-pack (PQFP) has been developed by using ANSYS™ finite element simulation code [1]. The model has been used for both thermo-mechanical stress analysis during temperature cycling and thermal characterization of the package under forced air cooling. Parametric studies have been performed on two different molding compounds with and without a drop-in heat spreader. In addition, the model has been simplified by substituting the leadframe and molding compound with a single homogeneous material, reflecting both molding compound and the leadframe thermo-physical properties. Results from the molding compound parametric studies indicate a lower package stress if the molding compound with low thermal expansion coefficient is used. Comparisons of principal and von Mises stresses show that the simplified model, overall, underpredicts the stresses. Although both the simplified and detailed models predict almost the same value for junction-to-case resistance (θ_{JC}), calculated values are significantly lower than the measured θ_{JC}. In contrast to θ_{JC}, the predicted junction-to-ambient resistances (θ_{JA}) are in good agreement with the measured data.

Introduction

One major trend in integrated circuit (IC) package design is the use of relatively large die in smaller packages [2]. These packages must be designed to avoid failure during fabrication, testing and operation. Since the electronic industry requires that the new products be introduced quickly into the market, the importance of analytical as well as numerical models becomes more pronounced for companies who want to stay at the leading edge of IC packaging technology. These models are used to provide a quantitative stress and thermal analysis for both existing and proposed new designs of complicated IC packages.

Although both the finite difference [3–5] and boundary element [4, 6] methods can be used for analysis of electronic packages, the finite element method (FEM) is the one most widely used in the electronic industry. A brief review of the applications of FEMs for thermal stress analysis is given in reference [7]. Several investigators used FEMs to predict stresses during temperature cycling. Lau [8] performed elasto-plastic analysis of thermal stresses and strains in a PQFP by using a three-dimensional finite element method. Materials used in the construction of the package were assumed to be elastic except the Sn/Pb solder which was assumed to be elasto-plastic due to its low yield strength, high ductility and linear strain-hardening characteristics. Lau [8] found that the stresses and strains in PQFP solder joint are smaller than those in plastic-leaded-chip-carrier (PLCC). Lau and Lian-Mueller [9] used finite element simulations for the optimization of hermetic package design. Three different designs were considered: (i) the package consisted of Ni-plated kovar lead frames, sealing glass ceramic body, Cu/Ag braze and tungsten, (ii) the same as (i) except that the Cu/Ag braze and the tungsten were eliminated, and (iii) the same as (i) except the device is connected to the tungsten metalization instead of the leads and the sealing glass. It was found that the stresses in the package given in (i) were greater than the ones described in (ii) and (iii). Simon et al. [10] performed parametric studies on plastic dual-in-line packages (PDIPs) for the predictions of thermally-induced stresses during die attach as well as after encapsulation by using a two-dimensional finite element model. Elevated thermal stresses were predicted near the center of the top layer of the chip for the die attach procedure. The superimposed results for the die attach and molding processes showed that the variations in both the die and package thickness have pronounced effect on the stress level; increased die thickness resulted in increased normal stress at the top of the chip. Charles and Clatterbaugh [11] carried out extensive finite element modeling and experimental testing to determine the optimum design parameters for solder joints in surface mount applications. Temperature cycling studies indicated joints with slightly higher standoffs and low fillet angles are more resistant to cycling fatigue than the pillar type joints.

In addition to thermally-induced stress analysis, FEMs are also widely used in thermal characterization of electronic packages. Cooke and Lee [12] used a three-dimensional finite element model for the thermal analysis of a 144 lead PQFP. Comparison of calculated temperature contours to that of

Contributed by the Electrical and Electronic Packaging Division for publication in the JOURNAL OF ELECTRONIC PACKAGING. Manuscript received by the EEPD August 1991.

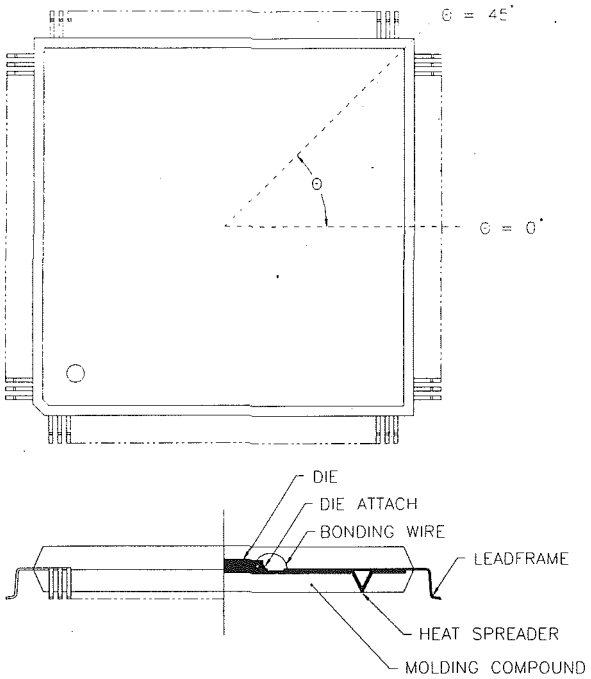

Fig. 1 Schematic of a high pin count PQFP

infrared picture showed similarity. Quantitatively, calculated results were higher than the experimental data. Childres and Peterson [13] determined individual thermal contact resistances and overall package resistance for an 18 lead PDIP by using a two-dimensional finite element model. It was found that the materials with thermal expansion coefficients below that of silicon tend to yield higher interface pressure, resulting in higher contact conductances than those achieved with expansion matched materials. Sweet and Cooley [14] presented an experimental and numerical characterization of the heat transfer for a 40 pin ceramic leadless chip carrier (CLCC) package and showed that the FEM calculations are useful in the study of qualitative features of the heat transport in convectively cooled packages. Aghazadeh and Mallik [15] predicted the thermal performance of a single and multi-layer 132 lead PQFP packages by using a three-dimensional finite element model. It was demonstrated that the package thermal resistance can be significantly reduced by using a multi-layer lead frame structure for medium and high lead count PQFP packages. Kozarek [16] compared FEM predictions of θ_{JC} with measurements in accordance with the SEMI and MIL standards. The measured case temperature was found to be significantly lower than the predicted temperature, therefore, detailed three-dimensional simulations were used to analyze thermocouple measurement problems in the region between the case and a cold plate. With the use of fiber-optic thermometry and surface-junction thermocouples, excellent agreement was obtained between measurements and predictions.

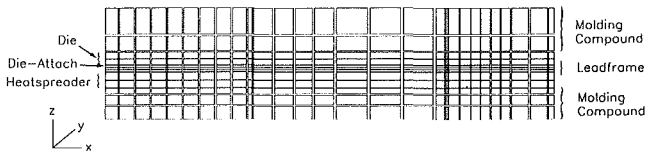

Fig. 2 Side view of finite element model at $\theta = 0$ symmetry plane

In the present study, a three-dimensional finite element model is used for the predictions of thermally-induced stresses under temperature cycling conditions. Finite element analysis is carried out for two different molding compounds with and without a drop-in heatspreader. The predicted stresses are compared for the selection of the molding compound which would result in lower stresses on the assembled package. The package with lower stresses is then used for thermal analysis. The calculated θ_{JC} and θ_{JA} values are compared with the measured data. In addition, stresses and thermal resistances obtained from both the simplified and detailed models are compared; conditions for the detailed and simplified models are discussed.

Finite Element Models

A finite element model of a high pin count PQFP is developed. The package is essentially flat and square in shape (28 mm wide, 28 mm long, and 3.6 mm thick). The silicon die is bonded to a 10.5 mm wide and 10.5 mm long leadframe platform (paddle) with a die attach epoxy. The leadframe and die assembly are encapsulated with a molding compound. A variation of this base case package includes a drop-in heatspreader below the leadframe as shown in Fig. 1. Package symmetry allows the package model to be a one octant section of the package. The model also includes the details of the leadframe.

The finite element model consists of 14,808 three-dimensional solid elements. Each element has 8 nodal points, each with three degrees of freedom (displacements in each coordinate direction) for the stress analysis and one degree of freedom (temperature) for the thermal analysis. Distinct material layers are divided into finer layers; three layers of molding compound below the drop-in heatspreader, two layers of heatspreader, two layers of leadframe, a single layer of die attach, two layers of silicon die, and two layers of molding compound above the die. For the package without a heatspreader, the heatspreader layers in the model are substituted with the molding compound. The side view of the finite element model at $y = 0$ (or $\theta = 0$ deg) symmetry plane is given in Fig. 2 for the package with a drop-in heatspreader. The elements are shrinked to indicate distinct finite elements. The finite element model of the leadframe is shown in Fig. 3.

In addition to the model described above, a simplified finite element model is also developed. This simplified model has 7272 three-dimensional brick elements compared to the 14,808 elements in the above detailed model. The simplified model differs from the detailed one with respect to the modeling of the leadframe. The leadframe and interlocking molding compound are assumed to be a homogeneous layer with 50 percent leadframe and 50 percent molding compound material thermo-

Nomenclature

A = surface area
c = specific heat
h = local heat transfer coefficient
$\bar{h}$ = averaged heat transfer coefficient
k = thermal conductivity
L = length
P = power
Pr = Prandtl number (Eq. (2))
Q = total convective heat transfer (Eq. (8))
Re = Reynolds number (Eq. (3))
T = temperature
V = coolant velocity
x = distance from the leading edge
θ_{JA} = junction-to-ambient resistance (Eq. (6))
θ_{JC} = junction-to-case resistance (Eq. (7))
μ = dynamic viscosity
ρ = density

Subscripts

A = ambient
C = case
J = junction
L = averaged over length
x = local value at x

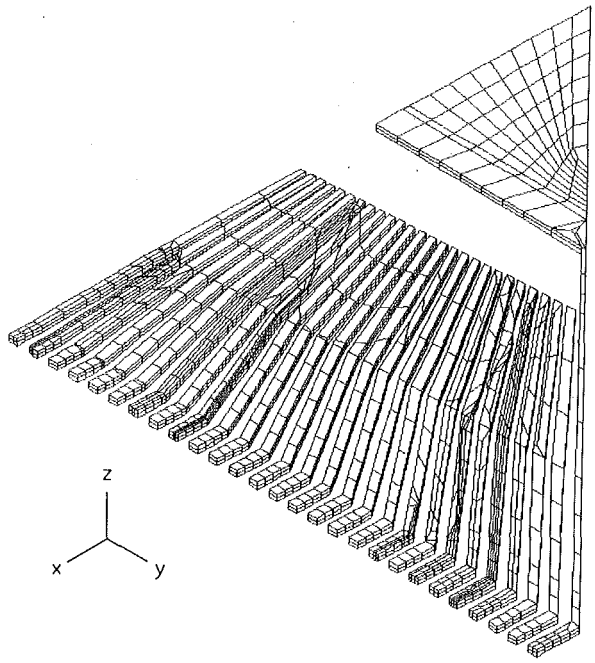

Fig. 3 Detailed finite element model of leadframe

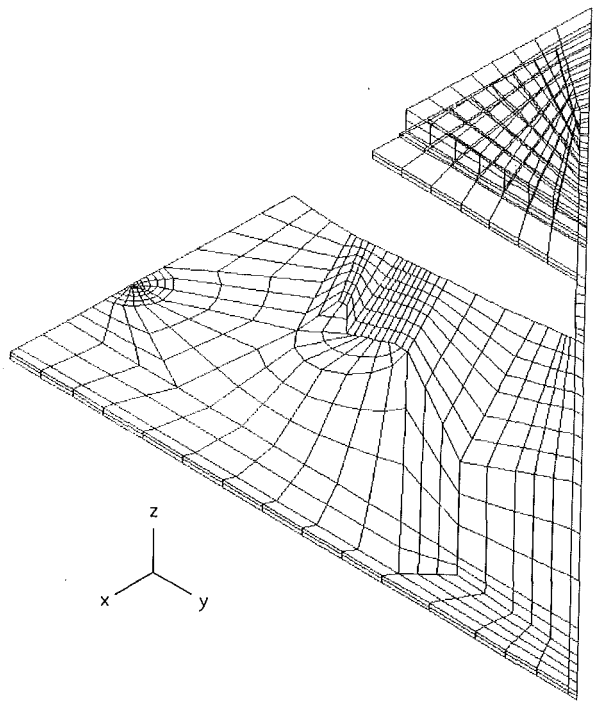

Fig. 4 Simplified leadframe and die assembly-finite element model

physical properties, eliminating the modeling details of the leads (see Fig. 4). Note that the actual leadframe material properties are used for the die pad and the support bar. Similar assumptions were used by Moore [3] in the characterization of a high thermal efficiency leadframe.

Material Properties

The material properties used for the stress and thermal analyses are given in Table 1. For the silicon die both ultimate tensile (UT) and compressive yield (CY) strength data are given in the table. These properties are obtained from CINDA's [17] and LSI Logic database [18] which is compiled from the vendor data. The material properties are assumed to be isotropic, linear elastic, and independent of temperature except thermal conductivity of the silicon.

Boundary and Initial Conditions

Steady-state, three-dimensional, linear elastic finite element analysis is performed for the prediction of thermally-induced stresses for packages constructed with different molding compounds and with and without a drop-in heatspreader. Since thermo-mechanical stresses are due to mismatches in thermal expansion coefficients of the materials used in the package construction, the lowest temperature in the cycle which is $-65°C$ is chosen to obtain the worst case stress levels.

The stress distribution depends on the selection of the stress free reference temperature and the amount of stress relaxation which occurs in the device. It is assumed that the stress free reference temperature is the curing temperature for the plastic encapsulation material (175°C). Since the purpose of this study is to compare two different molding compounds, the amount of stress relaxation is not an issue. Therefore, the package is assumed, initially, to be at 175°C and then is brought to the steady-state condition at $-65°C$.

In addition to the above assumptions, symmetry boundary conditions are also used. Since one octant section from the package (an angular cut from the center of the package between $\theta = 0$ deg to 45 deg planes) is used in FEM, displacements in θ directions are assumed to be zero at the symmetry planes ($\theta = 0$ and 45 deg).

Symmetry boundary conditions are also used on the planes of symmetry for thermal analysis where the adiabatic conditions (no heat flux across the symmetry plane) are used. In contrast to the stress analysis, ANSYS™ does not require explicit specification for an adiabatic heat flux boundary condition since it is a built in default boundary condition.

For both θ_{JC} and θ_{JA} evaluations, the package is initially assumed to be at equilibrium with an environment temperature of 20°C. Temperatures for the external nodes are specified at a constant value of 20°C for the junction-to-case resistance calculations. The ambient temperature is taken to be at 20°C for the junction-to-ambient resistance calculations. In addition to the ambient temperature specification, a specification for the convective heat transfer coefficient between the surface

Table 1 Material properties

Material property	Units	Molding compound A	Molding compound B	Die attach	Die	Leadframe	Heatspreader
Thermal conductivity	W/m-K	0.67	0.71	0.63		14.7	204.0
T = −25°C					191.0		
T = 25°C					148.0		
T = 75°C					119.0		
T = 125°C					98.9		
T = 225°C					76.2		
Young's modulus	kgf/mm^2	1150	1150	630	13300	14800	5630
Poisson's ratio		0.28	0.28	0.21	0.28	0.28	0.30
Thermal expansion coefficient	10^{-6} mm/mm-°C	13	15	57	1.4	4.3	24
Yield strength	kgf/mm^2	12.0	11.0	25.3	8.4 (UT) 510 (CY)	73.8	16.8

nodes and ambient is required. For the present study, only the forced convection cooling is considered to demonstrate the usefulness of a finite element modeling in package thermal characterization. Assuming a laminar flow over a flat plate, the local heat transfer coefficient, h_x, is obtained from [19, 20]

$$h_x = 0.332 \mathrm{Pr}^{1/3} \mathrm{Re}_x^{1/2} \left(\frac{k}{x}\right) \tag{1}$$

where k is the thermal conductivity of the coolant (e.g., for air cooling applications, k is the thermal conductivity of the air), Pr is the Prandtl number and Re is the Reynolds number. The dimensionless Prandtl and Reynolds numbers are defined

$$\mathrm{Pr} = \frac{\mu c}{k} \tag{2}$$

$$\mathrm{Re}_x = \frac{\rho V x}{\mu} \tag{3}$$

where V is the coolant velocity, x is the distance from the leading edge of the plate, μ, c, and ρ are the dynamic viscosity, the specific heat and the density of the coolant, respectively.

The local heat transfer coefficient correlation, Eq. (1), assumes a uniform surface temperature over the length of the plate. When this condition is not met, an average surface temperature must be used. Temperature dependent physical properties are evaluated at the bulk temperature, that is the average of the surface and ambient temperatures. In engineering applications, however, an averaged convective heat transfer coefficient is frequently used instead of a local heat transfer coefficient. The averaged heat transfer coefficient is obtained by integrating the local heat transfer coefficient over the surface area and then dividing the resultant value by the total surface area. Hence, the averaged convective heat transfer coefficient for laminar flow over a flat plate is obtained from

$$\bar{h}_L = 0.664 \mathrm{Pr}^{1/3} \mathrm{Re}_L^{1/2} \left(\frac{k}{L}\right) \tag{4}$$

where L is the total length of the flat plate. Ellison [21] showed that the thermo-physical properties of air slightly temperature dependent; the maximum error in 0°–100°C interval is less than 5 percent. Substituting the thermo-physical properties of air at temperature of 50°C into Eq. (4) gives the working correlation for practical engineering applications [21]

$$\bar{h}_L = 0.001092 \sqrt{V/L} \quad (\mathrm{W/in^2\text{-}°C}) \tag{5}$$

where V is the air velocity in ft/min and L is the total length in the flow direction in inches. For the present study, a 300 fpm air flow rate over a 1.102-in. square package is used for thermal analysis. Substituting the above values into Eq. (5) gives an estimated average heat transfer coefficient to be 0.018 W/in^2-°C (28 W/m^2-°C). This averaged heat transfer coefficient is assigned to all of the external elements of the finite element model.

Finally, a uniform heat generation value is assigned to the elements representing the silicon die. The silicon die is assumed to be generating a total of 11.6 W power which corresponds to the uniform volumetric heat generation of 0.34 W/mm^3 for a 9.2 mm square die with 0.41 mm thickness.

Experimental Procedure for Thermal Characterization

Determination of θ_{JC} and θ_{JA} require measurement of several primary parameters—junction temperature, case temperature, ambient air temperature, air flow rate and device power level. Among these parameters, the most difficult one to obtain is the junction temperature. This temperature can be obtained by using a special die which incorporates resistors and temperature sensitive diodes. An LSI Logic thermal test die is used in a PQFP package encapsulated with the selected molding compound. This thermal die consists of an interconnected array of 4.6 mm × 4.6 mm elements, each with resistive elements covering 95 percent of the surface area and five diodes positioned at the corners and at the center of the die for temperature sensing. The larger test die used in the PQFP is created by using a 2 by 2 array of a single test die. Each of the temperature sensing diodes on the test die is calibrated in a circulating bath of Fluorocarbon FC-40™ liquid maintained at a constant temperature. The calibration procedure and the thermal resistance testing are automated by using a Hewlett-Packard laboratory data acquisition system.

The package is surface mounted on a PC board with a hole corresponding to the center of the package where the thermocouple is attached to measure the surface (case) temperature. The whole assembly is immersed into a constant temperature, circulating bath of Fluorocarbon FC-40™ liquid. Power is then supplied to the test die. Power is raised in increments until a significant temperature difference is obtained between the junction and the case. After each power increase, the system is allowed to reach a steady-state condition (thermal equilibrium). During the entire test, the junction temperature, the case temperature and the coolant temperature are monitored. The junction temperature is obtained by using the diodes located at the center of the package. With the known supplied power (P) to the test die and the measured junction (T_J) and case (T_C) temperatures, the junction-to-case resistance (θ_{JC}) is obtained from [22]

$$\theta_{JC} = \frac{T_J - T_C}{P} \tag{6}$$

For junction-to-ambient resistance measurements, the PC board is inserted into a slot located in the fully developed region of the experimental wind tunnel. The inlet air velocity and bulk temperature are measured by pitot-static tube and thermocouples, respectively. As in the junction-to-case resistance measurements, the thermal resistance testing is automated by using Hewlett-Packard data acquisition system. During the entire test, the junction temperature, the ambient temperature and the air speed are monitored. With the known supplied power (P) to the test die and the measured junction (T_J) and ambient air (T_A) temperatures, the junction-to-ambient resistance (θ_{JA}) is calculated from [22]

$$\theta_{JA} = \frac{T_J - T_A}{P} \tag{7}$$

Results and Discussion

Stress Analysis. Three-dimensional stress and heat transfer analyses for a high pin count PQFP package with and without a drop-in heatspreader have been performed. The principal and von Mises stresses were obtained from the finite element solution under temperature cycling conditions by using a simplified finite element model. Thermo-mechanical stresses were obtained at −65°C. The predicted stresses along with the warpage on the package are summarized in Table 2. For comparison, the results obtained with the detailed model for Case 3 are also presented in Table 2 (see Case 5). In addition, the predicted results for the package with the lowest stresses are used to normalize the data given in Table 2. The heatspreader layer, however, was normalized by using the results obtained for the package constructed with the molding compound B; results are shown in Table 3. The overall package results are summarized in the first row of each case studied. Since these results are obtained by averaging displacements and stresses across dissimilar materials, the averaged data may be misleading. Therefore, displacements and stresses are also given in Tables 2 and 3 for individual material layers.

Comparison of the simplified model results, Cases 1 through 4, given in Tables 2 and 3 clearly indicates that the package

Table 2 Maximum stresses and warpage

Construction type and layers	σ_1 (kgf/mm^2)	σ_3 (kgf/mm^2)	σ_E (kgf/mm^2)	Warpage (mm)
Case 1 (base case, simplified model)				
Molding compound A without heatspreader	11.43	−57.09	58.25	0.057
Molding compound	7.09	− 7.69	11.20	0.057
Die	3.90	−30.92	26.89	0.013
Die attachment	13.68	− 3.28	13.94	0.015
Leadframe	11.43	−64.25	59.00	0.053
Case 2 (simplified model)				
Molding compound B without heatspreader	12.78	−68.84	70.23	0.065
Molding compound	9.11	− 8.52	12.67	0.065
Die	4.46	−35.74	30.68	0.015
Die attachment	14.00	−4.69	15.36	0.016
Leadframe	12.78	−77.47	71.01	0.059
Case 3 (simplified model)				
Molding compound A with heatspreader	26.54	−72.54	68.59	0.123
Molding compound	7.05	−12.23	14.55	0.123
Die	6.43	−43.23	37.62	0.030
Die attachment	14.92	−6.21	17.30	0.032
Leadframe	11.49	−80.89	73.73	0.120
Heatspreader	33.03	−9.10	30.01	0.100
Case 4 (simplified model)				
Molding compound B with heatspreader	25.48	−78.61	74.23	0.117
Molding compound	9.07	−12.74	15.76	0.117
Die	6.99	−46.03	40.02	0.031
Die attachment	15.22	−7.74	18.81	0.032
Leadframe	12.78	−87.89	79.50	0.114
Heatspreader	31.75	−8.67	29.29	0.096
Case 5 (detailed model)				
Molding compound A with heatspreader	26.09	−67.20	69.05	0.123
Molding compound	8.57	−13.19	15.27	0.123
Die	23.62	−19.24	46.15	0.031
Die attachment	17.62	−10.29	18.20	0.033
Leadframe	29.50	−88.31	70.01	0.119
Heatspreader	32.71	−19.04	33.61	0.101

Table 3 Normalized Stresses and Warpage

Construction Type and Layers	$\sigma_1/\sigma_{1,\text{ref}}$	$\sigma_3/\sigma_{3,\text{ref}}$	$\sigma_E/\sigma_{E,\text{ref}}$	$\delta/\delta_{\text{ref}}$
Case 1 (base case, simplified model)				
Molding compound A without heatspreader	1.00	1.00	1.00	1.00
Molding compound	1.00	1.00	1.00	1.00
Die	1.00	1.00	1.00	1.00
Die attachment	1.00	1.00	1.00	1.00
Leadframe	1.00	1.00	1.00	1.00
Case 2 (simplified model)				
Molding compound B without heatspreader	1.12	1.21	1.21	1.14
Molding compound	1.28	1.11	1.13	1.14
Die	1.14	1.16	1.14	1.15
Die attachment	1.02	1.43	1.10	1.07
Leadframe	1.12	1.21	1.20	1.11
Case 3 (simplified model)				
Molding compound A with heatspreader	2.32	1.27	1.18	2.16
Molding compound	0.99	1.59	1.30	2.16
Die	1.65	1.40	1.40	2.31
Die attachment	1.09	1.89	1.24	2.13
Leadframe	1.01	1.26	1.25	2.26
Heatspreader	(1.04)	(1.05)	(1.02)	(1.04)
Case 4 (simplified model)				
Molding compound B with heatspreader	2.23	1.38	1.27	2.05
Molding compound	1.28	1.66	1.41	2.05
Die	1.79	1.49	1.49	2.38
Die attachment	1.11	2.36	1.35	2.13
Leadframe	1.12	1.37	1.35	2.15
Heatspreader	(1.00)	(1.00)	(1.00)	(1.00)
Case 5 (detailed model)				
Molding compound A with heatspreader	2.28	1.18	1.19	2.16
Molding compound	1.21	1.72	1.36	2.16
Die	6.06	0.62	1.72	2.38
Die attachment	1.29	3.14	1.31	2.20
Leadframe	2.58	1.37	1.19	2.25
Heatspreader	(1.03)	(2.20)	(1.15)	(1.05)

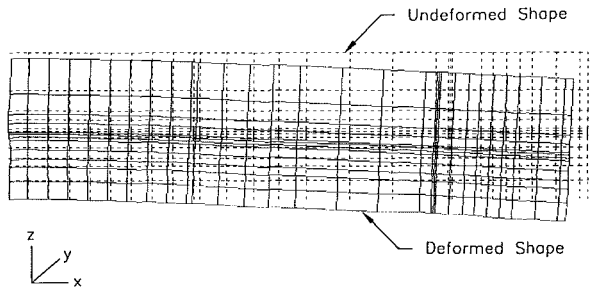

Fig. 5 Deformation of PQFP assembly at θ = 0 symmetry plane

molded with the compound A and without heatspreader has less thermal stress and warpage than the other packages. Examination of the data further indicates that the maximum stress takes place in the leadframe for all of the cases studied. When the results of the simplified and detailed models, Cases 3 and 5, are compared, it is seen that the simplified model generally underpredicts von Mises stresses in all of the material layers except the leadframe. The larger discrepancy occurs in the die layer where the underprediction is about 28 percent. The simplified model predicts higher compressive principal stresses on the die whereas higher tensile principal stresses are obtained from the detailed model. Although the stresses predicted from both models differ significantly, the predicted warpages are in good agreement (see Tables 2 and 3). Due to the similarity in predicted results from both the simplified and detailed models, the selected plots from the Case 5 study (detailed model) are presented.

The predicted deflections (warpage) of the PQFP assembly at the θ = 0 deg symmetry plane are shown in Fig. 5. The dotted lines are for the original assembly and the solid lines are for the displaced assembly. It can be seen that the whole package bends downwards. This is due to the mismatch in

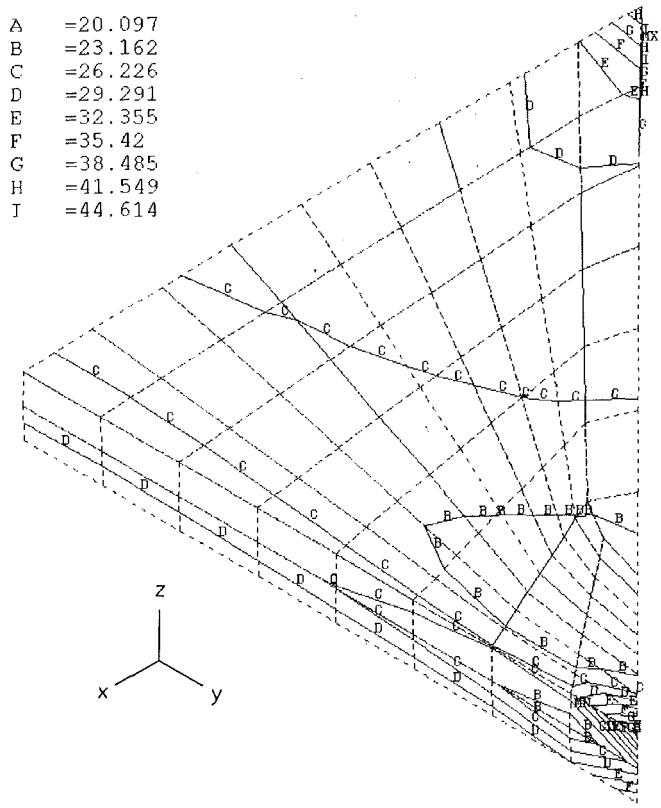

Fig. 6 Von Mises stress contours on the top surface of the die

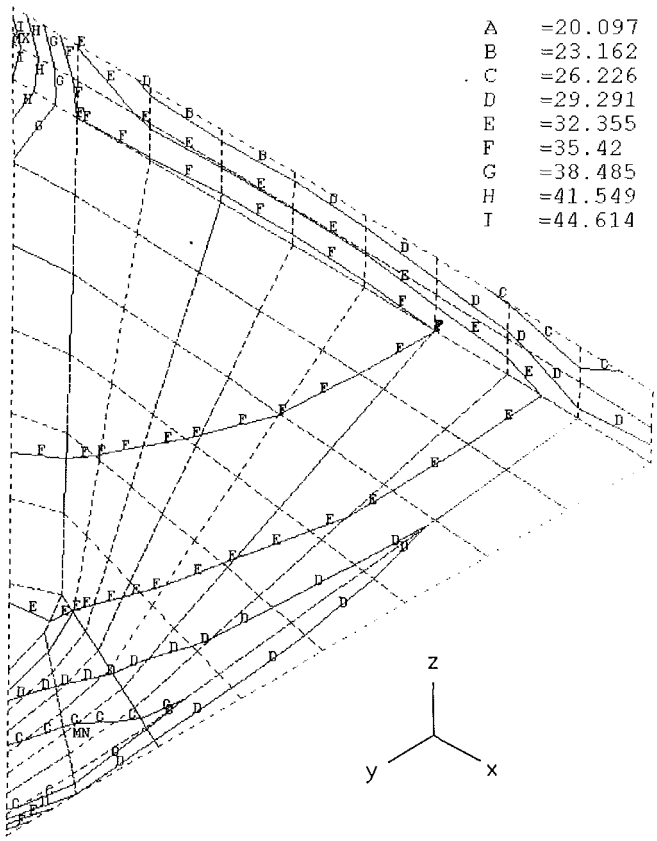

Fig. 7 Von Mises stress contours on the bottom surface of the die

thermal expansion coefficients and stiffness between all parts of the PQFP assembly. The maximum bending takes place at the edge of the package which is about 3 percent of the total package thickness.

The von Mises stress contours on the top and bottom surfaces of the die are shown in Figs. 6 and 7. It is seen that the higher stresses occur at the corner and at the center of the die. The stresses on the bottom surface of the die are about 15 percent higher than the stresses on the top surface. Since the maximum stress occurs at the corner of the silicon die, failure of the package could happen there during temperature cycling. In that case, further crack propagation in the molding compound is likely. Consequently, moisture could enter through the crack and affect the package reliability.

Figure 8 shows the von Mises stress distribution on the top surface of the die attach material where adhesion to the die surface takes place. It is seen that higher stresses are attained at the region corresponding to the outer edge of the die. Since the die attach serves a buffer zone between the die and the leadframe, the stresses created on the die are absorbed by the die attach material. Lower Young's modulus of the die attach suggests that the material would go under plastic deformation. The present study does not consider plastic deformation.

As shown in Fig. 9, the highest stress in the leadframe is obtained at the die pad support bar. Higher stresses are also predicted in the region where the metallic contact between the leads and heatspreader takes place. The footprint of the heatspreader is clearly seen by the stress distribution patterns as shown in Fig. 9. As pointed out earlier, the highest stress in the overall package is predicted within the leadframe (see Tables 2 and 3).

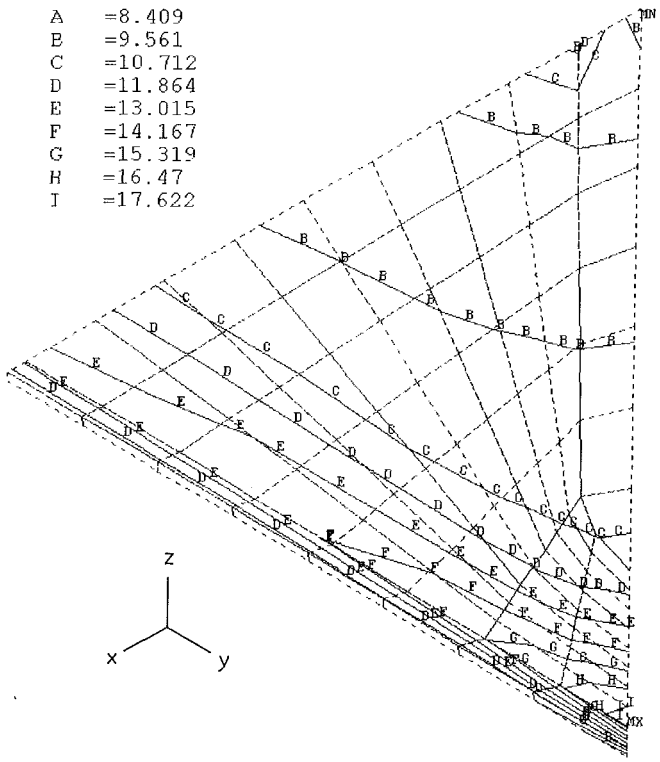

Fig. 8 Von Mises stress contours on the top surface of die-attach

Thermal Analysis. The molding compound which resulted in lower package stress was chosen for the thermal analysis. The junction-to-case and junction-to-ambient resistances have been determined from the finite element analysis. Comparisons of the predicted results with the measured data are given in Table 4. Subscripts "p" and "m" denote the predicted and measured data, respectively. Numbers enclosed within parantheses indicate percentage deviation from the measured data.

Steady-state temperature distribution within the package is obtained from a finite element analysis (FEA) for specified

Table 4 Predicted and measured θ_{JC} and θ_{JA} values for molding compound A

Simulations	T_J (°C)	T_C (°C)	T_A (°C)	$(\theta_{JC})_p/(\theta_{JC})_m$ (°C/W)	$(\theta_{JA})_p/(\theta_{JA})_m$ (°C/W)
Simplified model without heatspreader					
Constant case temperature	125.82	20.0	N/A	9.12/(11.0) (−17.1%)	N/A
Air speed = 300 fpm	570.49	N/A	20.0	N/A	47.46/41.3 (14.9%)
Simplified model with heatspreader					
Constant case temperature	55.86	20.0	N/A	3.09/6.8 (−54.6%)	N/A
Air speed = 300 fpm	283.70	N/A	20.0	N/A	22.73/23.4 (−2.9%)
Detailed model with heatspreader					
Constant case temperature	55.90	19.96	N/A	3.10/6.8 (−54.4%)	N/A

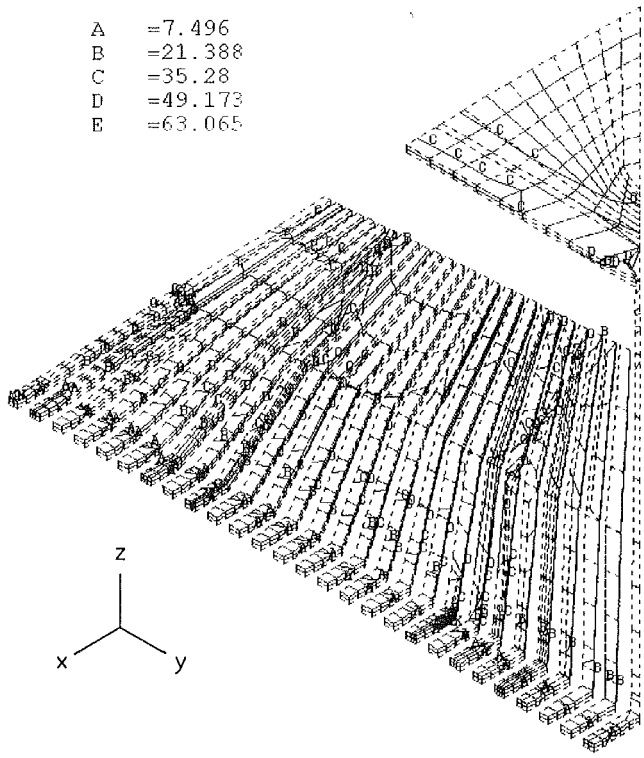

Fig. 9 Von Mises stress contours on the top surface of leadframe

boundary conditions and volumetric heat generation. The predicted maximum temperature (junction temperature of the die) is reported in Table 4 along with the specified case and ambient temperatures. θ_{JC} and θ_{JA} are obtained by using Eqs. (6) and (7) and the known junction temperature, power generation, case temperature and bulk ambient temperature. These calculated values are given in Table 4.

Comparisons of both the predicted and measured results clearly indicate that the package with a drop-in heatspreader has lower thermal resistances than the one without a drop-in heatspreader. For example, the θ_{JC} value predicted from the FEA dropped about 66 percent when a drop-in heatspreader was added to the package. The reduction in the measured θ_{JC} is found to be about 38 percent. Similarly, the drop in θ_{JA} value with the addition of the heatspreader is found to be 52 percent and 43 percent for the predicted and measured data, respectively. On the other hand, the predicted θ_{JC} values from the simplified and detailed models are found to be in good agreement (see Table 4).

The comparison of the predicted and measured θ_{JC} values indicates significant difference; the predicted θ_{JC} is about 55 percent of the measured one. Similar pattern has been reported in the literature [12, 14, 16, 23]. This discrepancy might be due to possible error in thermal conductivity values used in the analysis and the differences in the constant wall temperature boundary conditions used in the simulation and experiment. If we exclude the material properties as the major source for the discrepancy, then the measured data becomes questionable. Lee and Sen [28] found that the predicted junction-to-case resistance from FEA for the TQFP (Tape Quad Flat Pack) package was significantly higher than the measured data. This difference is attributed to the constant temperature boundary condition imposed during experiment. Thermal bath measurements are especially sensitive to error; the constant surface temperature is not easy to maintain during the measurement due to the boundary layer development in the vicinity of the package surface. Sweet and Cooley [14] reported similar observations and also pointed out that the placement of the thermocouple in the epoxy is of critical importance to the thermocouple reading. Lee and Sen [28] added a thin fluid boundary layer on the surface of the package in the finite element model so that the predicted θ_{JC} could approach to the measured value. It was found that the added liquid boundary layer thickness must be at least 0.06 cm to match the predicted results with the measured ones. Beyond 0.06 cm boundary layer thickness, there is no significant difference observed between the measured and predicted θ_{JC} values.

Although the discrepancy in the θ_{JC} value is large, the θ_{JA} prediction is not affected by the error in θ_{JC} (see Table 4). For the θ_{JA} calculation, the external effects (fluid velocity and bulk temperature) are more significant than the material property effects; therefore, the predicted values are closer to the experimental values (3 and 14 percent difference in the package with and without a drop-in heatspreader, respectively).

Since the predicted values from both the simplified and detailed models are in good agreement, the results obtained from the simplified model are presented. Figures 10 and 11 show the developed temperature contours under steady-state condition for the packages simulated in a thermal bath with a constant temperature of 20°C. The package is initially assumed to be at the thermal equilibrium with the bath fluid. The constant surface temperature condition can be also thought to be the case of air cooling with an infinite (very large) air speed, that is the case when the convective heat transfer coefficient approaches infinity while the case and ambient temperature difference approaches to zero. This can also be deduced from

$$Q = hA(T_C - T_A) \tag{8}$$

where Q is the total amount of heat flux from the package surface (dissipated heat) in Watts, h is the convective heat transfer coefficient in W/m^2-°C, A is the total external surface area in m^2, and T_C and T_A are the case and bulk ambient temperatures, respectively. For a finite value of total heat dissipation (Q), $h \rightarrow \infty$, when $T_C = T_A$. As the air speed approaches infinity, convective heat transfer coefficient ap-

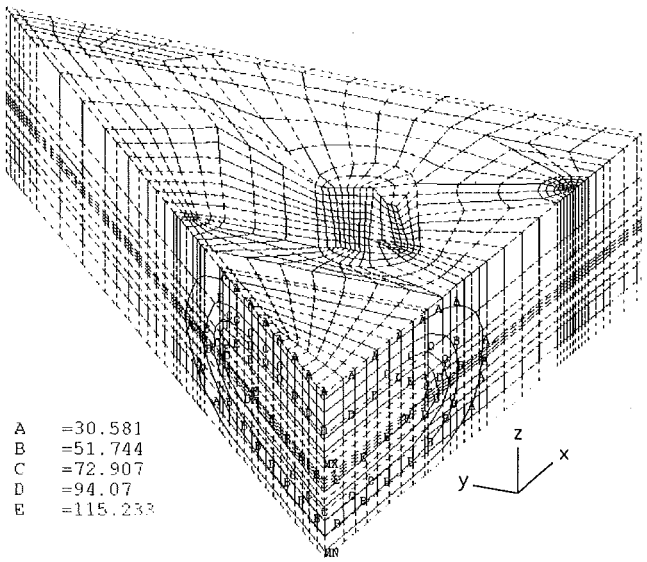

Fig. 10 Temperature contours for the package without drop-in heatspreader (T_c = 20°C)

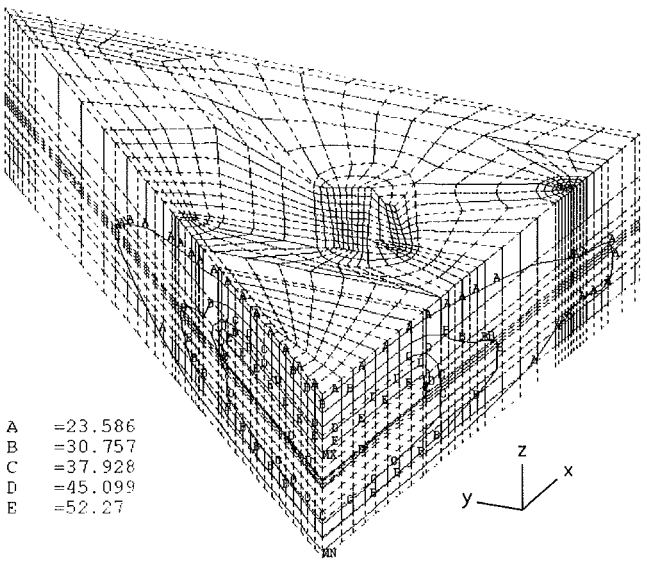

Fig. 11 Temperature contours for the package with drop-in heatspreader (T_c = 20°C)

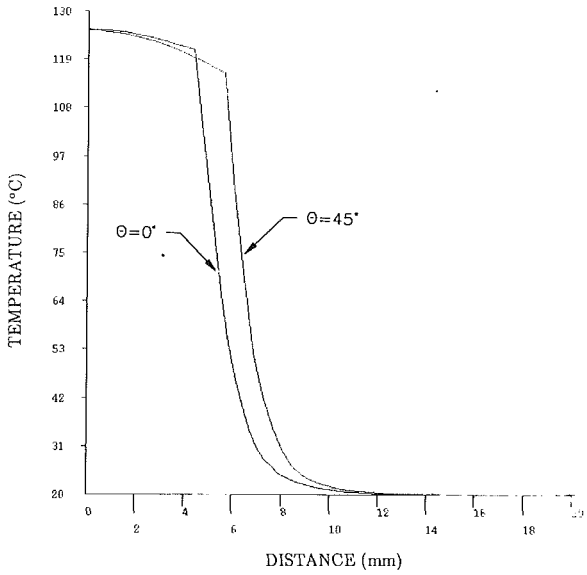

Fig. 12 Temperature distributions along the symmetry planes corresponding to the center of die (without drop-in heatspreader, T_c = 20°C)

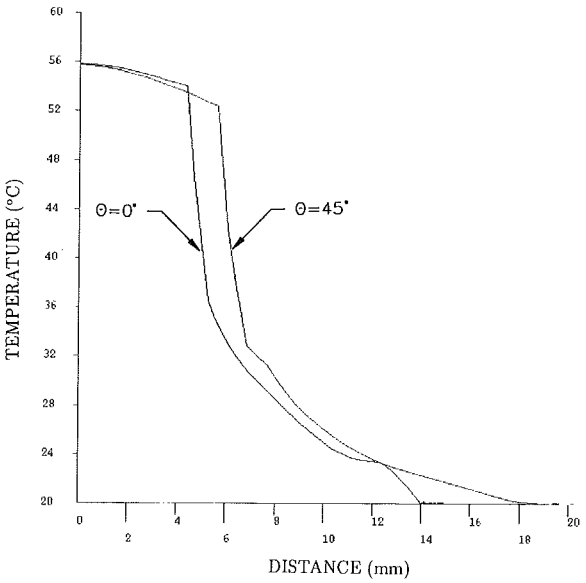

Fig. 13 Temperature distributions along the symmetry planes corresponding to the center of die (with drop-in heatspreader, T_c = 20°C)

proaches infinity for a given finite package length—see Eq. (5).

Figure 10 indicates that the maximum temperature for the package without a heatspreader is obtained within the center region of the silicon which is about 125°C. Since the package length is much greater than the thickness, the significant heat transfer takes place in the direction of the smaller dimension where there is less resistance to the heat flux. It is interesting to note that the effect of heating on the molding compound at the symmetry planes (θ = 0 and 45 deg) is confined into a smaller region; beyond this region there is no heating effect. The region that is affected by the heating is called the thermal penetration depth. This thermal penetration depth is smaller in low thermal conductivity material (for example, thermal conductivity of the molding compound is about one-hundreth of the silicon). When a drop-in heatspreader is used in the package, the heating effect is moved towards the edge of the package resulting in a longer thermal penetration depth as shown in Fig. 11. Therefore, the drop-in heatspreader provides better thermal management by reducing the junction temperature about 56 percent from the case without a heatspreader (see Table 4).

The thermal penetration effect can be clearly seen from the temperature profiles given in Figs. 12 and 13 for packages with and without a drop-in heatspreader, respectively. These temperatures are obtained along the symmetry planes (θ = 0 deg and θ = 45 deg) at the elevation corresponding to the midplane of the silicon. It is seen that the temperature varies slightly within the silicon die, suggesting a uniform temperature distribution (refer Figs. 12 and 13 for the temperature distribution between 0 and 4.6 mm). Figure 12 indicates that the temperatures start to drop suddenly within a narrow region at the silicon edge corresponding to the thermal penetration depth length; beyond this region (beyond 10 mm) temperature stays constant. For this case, the thermal penetration depth is about one-third of the package length (note that the package length in θ = 0 direction is 14 mm, and the thermal penetration depth, δ_t = 10 − 4.5 = 5.5 mm). The length of the thermal penetration depth or the heat spreading effect increases if the heat-

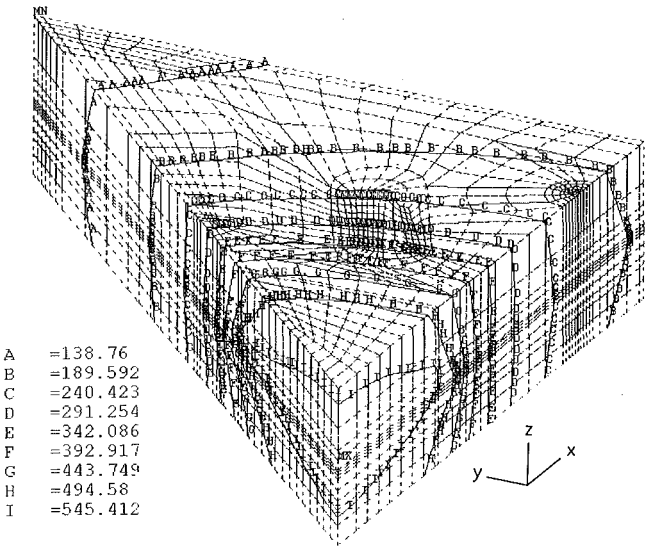

Fig. 14 Temperature contours for the package without drop-in heatspreader (T_a = 20°C and v_{air} = 300 fpm)

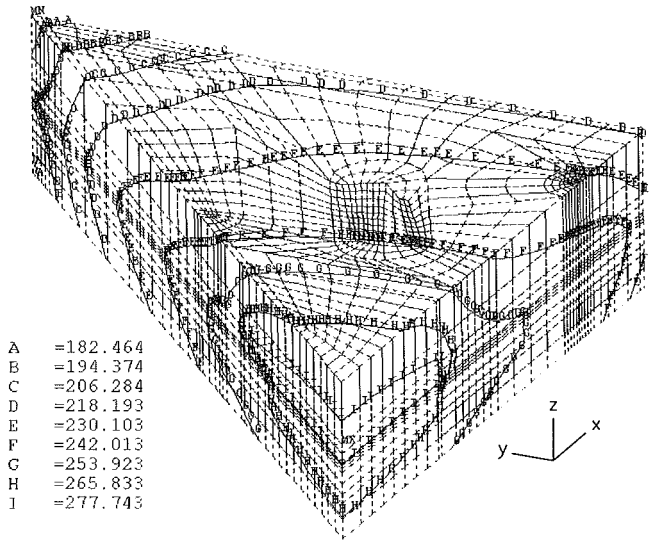

Fig. 15 Temperature contours for the package with drop-in heatspreader (T_a = 20°C and v_{air} = 300 fpm)

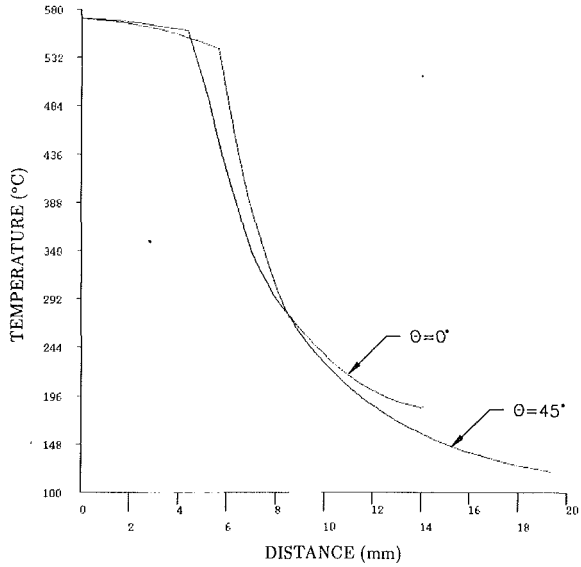

Fig. 16 Temperature distributions along the symmetry planes corresponding to the center of die (without drop-in heatspreader, T_a = 20°C and v_{air} = 300 fpm)

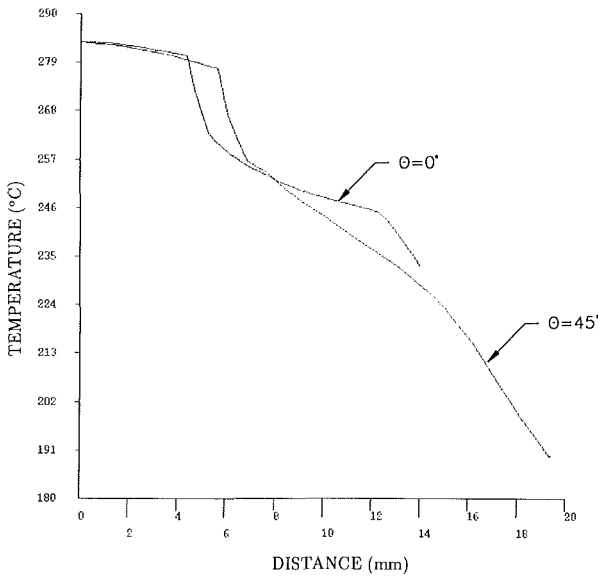

Fig. 17 Temperature distributions along the symmetry planes corresponding to the center of die (with drop-in heatspreader, T_a = 20°C and v_{air} = 300 fpm)

spreader is employed (see Fig. 13, where the heating effect reaches to the package edge).

Simulations are also performed for thermal characterization of packages under forced air cooling. For demonstration purposes, an air speed of 300 fpm is selected and the bulk ambient temperature is taken to be 20°C. The convective heat transfer coefficient obtained from Eq. (5) is assigned to the elements at the package surface. The predicted steady-state results are shown in Figs. 14 and 15 for the packages without and with a drop-in heatspreader, respectively. Corresponding temperature plots along the symmetry planes are given in Figs. 16 and 17. For the given heat dissipation, surface area, and ambient temperature, the case temperature is inversely proportional with the heat transfer coefficient—see Eq. (8). As the heat transfer coefficient decreases, the case temperature increases which in turn results in a higher junction temperature. Therefore, the predicted junction temperatures are higher than the previously obtained values (constant case temperature)—see Table 4. The predicted junction temperatures are much higher than the allowable junction temperature (125–150°C), suggesting inefficient cooling of the package. Note that the junction temperature is reduced about 50 percent with the heatspreader. Further reduction could be achieved by using an external heat sink or providing higher air flowrates for the package with a drop-in heatspreader.

Conclusions

A finite element thermal and stress analysis of a high pin count PQFP has been presented in this paper. The stress and temperature distributions for a best configured package have also been provided to better understand the mechanical and thermal behavior of the package.

Two different molding compounds were evaluated for a PQFP with and without a drop-in heatspreader under temperature cycling conditions. The package with lower stresses was evaluated for thermal characteristics. Based on the comparisons made, molding compound A, which has a lower thermal expansion coefficient than the molding compound B, is the best suitable for a high pin count PQFP. The von Mises stresses within the package are highest in the leadframe and

the lowest in the molding compound. Comparisons of the simplified and the detailed model predictions indicate that the simplified model underpredicts von Mises stresses. If the magnitude of stress levels are important, then it is suggested that the finite element model should include all the relevant package details. On the other hand, if the trend or comparison studies are required, then the finite element model should be as simple as possible.

Based on the thermal analysis of the PQFP packages, the package with a drop-in heatspreader performs better than the one without a heatspreader. Under constant temperature (20°C) immersion cooling, the junction temperature of the device with a heatspreader is about 45 percent of the temperature obtained for a standard package without a heatspreader. Similar results are obtained under forced air cooling conditions. The results also indicate that the selected air speed for the analysis is not adequate to dissipate 11.6W from the device within the required junction temperature limitations. Further improvement is possible by using higher air flow rates combined with an external heat sink. Comparison of the detailed and simplified model results indicates that the predictions from both models are in good agreement, suggesting that the model for thermal analysis does not require as much detail as for the model used for stress analysis.

Comparisons of experimental and the predicted values indicate good agreement for θ_{JA} values but large deviations for θ_{JC} values. The predicted values from the FEA are lower than the measured θ_{JC} values.

The observed difference in the predicted and measured θ_{JC} value can be attributed, first, to the possible error in the thermal conductivity data used in the analysis and, second, to the measurement errors. The finite element model differs from the experiment in terms of the specification of constant case temperature. In general, it is difficult to maintain a constant temperature in the vicinity of the package. Due to the heat dissipation through the package, the thin boundary layer could form adjacent to the package surface resulting in inefficient cooling of the package. This would in turn result in a higher junction temperature.

The present analysis shows that finite element is a viable tool for optimizing design to reduce package stress and for determining thermal management options to maintain the device within an allowable operating temperature limit. The results presented here should be especially valuable to packaging engineers in the design of plastic packages.

Acknowledgments

The author is very pleased to acknowledge Dr. B. K. Sen and Mr. K. Newman of LSI Logic Corporation for stimulating technical discussions on this subject and for their constructive comments which led to the improvement of this paper.

References

1 *ANSYS™ Engineering Analysis System User's Manual*, Swanson Analysis Systems, Inc., Houston, Pa, May 1989.

2 Pinnel, M. R., and Knausenberger, W. H., "Interconnection System Requirement and Modeling," in *Electronic Materials Handbook, Vol. 1: Packaging*, ASM International, Materials Park, Ohio, 1989, pp. 12–17.

3 Moore, T., "The Design and Characterisation of a High Thermal Efficiency Leadframe with an Integral Heatspreader," *Proc. of the 7th IEEE Semi-Therm Symposium*, Phoenix, Arizona, Feb. 12–14, 1991, pp. 98–104.

4 Wright, J. L., Marks, B. W., and Decker, K. D., "Modeling of MMIC Devices for Determining MMIC Channel Temperatures During Life Tests," *Proc. of the 7th IEEE Semi-Therm Symposium*, Phoenix, Ariz., Feb. 12–14, 1991, pp. 131–139.

5 Yokono, Y., and Ishizuka, M., "Thermal Studies on Finned LSI Packages Under Forced Convection," *Proc. of the 5th IEEE Semi-Therm Symposium*, San Diego, Calif., Feb. 7–9, 1989, pp. 20–24.

6 Liu, J. C., Hunter, D. E., and Kozarek, R. L., "Electronic Package Thermal Design Using Boundary Elements," *Proc. of the 6th IEEE Semi-Therm Symposium*, Phoenix, Ariz., Feb. 6–8, 1990, pp. 65–69.

7 Simon, B. R., Staszak, Z. J., Prince, J. L., Yuan, Y., and Umaretiya, J. R., "Improved Finite Element Models of Thermal/Mechanical Effects in VLSI Packaging," *Proc. of the 8th Annual International Electronics Packaging Conference*, Dallas, Texas, Nov. 6–10, 1988.

8 Lau, J. H., "Thermal Stress Analysis of SMT PQFP Packages and Interconnectors," ASME JOURNAL OF ELECTRONIC PACKAGING, Vol. 111, 1989, pp. 2–8.

9 Lau, J. H., and Lian-Mueller, L. B., "Finite Element Modeling for Optimizing Hermetic Package Reliability," ASME JOURNAL OF ELECTRONIC PACKAGING, Vol. 111, 1989, pp. 255–260.

10 Simon, B. R., Yuan, Y., Umaretiya, J. R., Prince, J. L., and Staszak, Z. J., "Parametric Study of a VLSI Plastic Package Using Locally Refined Finite Element Models," *Proc. of the 5th IEEE Semi-Therm Symposium*, San Diego, Calif., Feb. 7–9, 1989, pp. 52–58.

11 Charles, H. K., Jr., and Clatterbaugh, G. V., "Solder Joint Reliability—Design Implications From Finite Element Modeling and Experimental Testing," ASME JOURNAL OF ELECTRONIC PACKAGING, Vol. 112, 1990, pp. 135–146.

12 Cooke, J. A., and Lee, S. W., "Finite Element Thermal Analysis of 144 Pin Plastic Flat Packs," *Proc. of the 5th IEEE Semi-Therm Symposium*, San Diego, Calif., Feb. 7–9, 1989, pp. 59–62.

13 Childres, W. S., and Peterson, G. P., "Quantification of Thermal Contact Conductance in Electronic Packages," *Proc. of the 5th IEEE Semi-Therm Symposium*, San Diego, Calif., Feb. 7–9, 1989, pp. 30–36.

14 Sweet, J. W., and Cooley, W. T., "Thermal Resistance Measurements and Finite Element Calculations for Ceramic Hermetic Packages," *Proc. of the 6th IEEE Semi-Therm Symposium*, Phoenix, Ariz., Feb. 6–8, 1990, pp. 10–16.

15 Aghazadeh, M., and Mallik, D., "Thermal Characteristics of Single and Multi-Layer High Performance PQFP Packages," *Proc. of the 6th IEEE Semi-Therm Symposium*, Phoenix, Ariz., Feb. 6–8, 1990, pp. 33–39.

16 Kozarek, R. L., "Effect of Case Temperature Measurement Errors on the Junction-to-Case Thermal Resistance of a Ceramic Package," *Proc. of the 7th IEEE Semi-Therm Symposium*, Phoenix, Ariz., Feb. 12–14, 1991, pp. 44–51.

17 Desai, P. D., et al., "Thermal, Physical, Electrical, Mechanical, and Other Properties of Selected Packaging Materials," prepared for Semiconductor Research Corporation (16 volumes published as of May 1992).

18 Mertol, A., "Thermal/Mechanical/Electrical Material Database," LSI Logic Internal Report, Feb. 1991.

19 Rohsenow, W. M., and Choi, H., *Heat, Mass, and Momentum Transfer*, Prentice-Hall, Inc., Englewood Cliffs, New Jersey, 1961, p. 148.

20 Moffat, R. J., and Ortega, A., "Direct Air Cooling of Electronic Components," *Advances in Thermal Modeling of Electronic Components and Systems*, ed. by A. Bar-Cohen and A. D. Kraus, Hemisphere Publishing Corporation, New York, New York, Vol. 1, 1988, pp. 129–282.

21 Ellison, G. N., *Thermal Computations for Electronic Equipment*, Reprint Edition, Robert E. Krieger Publishing Company, Malabar, Florida, 1989, pp. 48–49.

22 Hannemann, R., Fox, L. R., and Mahalingham, M., "Thermal Design for Microelectronic Components," *Cooling Techniques for Computers*, ed. by W. Aung, Hemisphere Publishing Corporation, New York, New York, 1991, pp. 245–276.

23 Lee, A., and Sen, B. K., "Thermal Simulation of Pill Package," *Technical Conference Proceedings*, LSI Logic Corporation, Milpitas, California, Oct. 16–21, 1988.